Journal of Magnetic Resonance **156,** 262–268 (2002)
doi:10.1006/jmre.2002.2537

Novel 2D Triple-Resonance NMR Experiments for Sequential Resonance Assignments of Proteins

Keyang Ding and Angela M. Gronenborn[1]

Laboratory of Chemical Physics, National Institute of Diabetes and Digestive and Kidney Diseases, National Institutes of Health, Bethesda, Maryland 20892

Received January 17, 2002; revised March 19, 2002; published online June 20, 2002

We present 2D versions of the popular triple resonance HN(CO)CACB, HN(COCA)CACB, HN(CO)CAHA, and HN(COCA)CAHA experiments, commonly used for sequential resonance assignments of proteins. These experiments provide information about correlations between amino proton and nitrogen chemical shifts and the α- and β-carbon and α-proton chemical shifts within and between amino acid residues. Using these 2D spectra, sequential resonance assignments of H^N, N, C^α, C^β, and H^α nuclei are easily achieved. The resolution of these spectra is identical to the well-resolved 2D ^{15}N–^1H HSQC and H(NCO)CA spectra, with slightly reduced sensitivity compared to their 3D and 4D versions. These types of spectra are ideally suited for exploitation in automated assignment procedures and thereby constitute a fast and efficient means for NMR structural determination of small and medium-sized proteins in solution in structural genomics programs.

Key Words: **proteins; sequential assignment; reduced dimensionality; structural genomics.**

INTRODUCTION

Multidimensional (3D and 4D) NMR experiments (*1, 2*) have been routinely applied in solution structure determination of uniformly ^{15}N, ^{13}C isotope labeled proteins. Although very powerful, high-dimensionality spectra have several drawbacks that render them less desirable than 2D spectra for purposes of fast, automated analyses. In particular, short, maximal evolution times in one (in the case of 3D) or two (in the case of 4D) of the dimensions have to be tolerated, resulting in large uncertainties in the accuracy of chemical shifts. This necessitates a rather large error tolerance to be set in peak picking and merging–matching algorithms (*3–5*), frequently yielding too many possible assignments. In addition, the data sizes of 4D experiments can become extremely large, at least one or two orders greater than 2D experiments recorded with identical sweep widths, creating enormous demands for instrument time, if used on a routine basis. It therefore is desirable to develop alternative approaches without compromising resolution or sensitivity. In that respect, a number of reports on reduced dimensionality experiments have appeared (*6–13*) that can be used to overcome some of the problems. Such experiments provide correlations of n chemical shifts in $n-1$ dimensional spectra, greatly reducing experimental time and data size while retaining identical correlation information to their parent counterparts. The associated pulse sequences employ the accordion principle (*14*), incorporating two evolution frequencies into a common dimension, with one frequency splitting the second one. Based on this general notion, we decided to reduce the dimension of all standard n dimensional (3D and 4D) experiments that exploit scalar connectivities into $n-2$ dimensional experiments. Theoretically, it is easily possible to incorporate three evolution frequencies into a common dimension, using two frequencies to split the third one. To the best of our knowledge, however, no such reports have appeared in the literature and no 2D experiments correlating four or more chemical shifts are in use.

For sequential assignments of proteins, the magnetization transfer pathway H $\leftrightarrow$ N $\leftrightarrow$ CO $\leftrightarrow$ CA via heteronuclear J couplings is highly efficient and exhibits good sensitivity. In contrast, the magnetization transfer efficiency for the scalar pathway H $\leftrightarrow$ N $\leftrightarrow$ CA $\leftrightarrow$ CO is substantially lower. Likewise, magnetization transfer for H $\leftrightarrow$ N $\leftrightarrow$ CA $\leftrightarrow$ CB is significantly better than for H $\leftrightarrow$ N $\leftrightarrow$ CA $\leftrightarrow$ CO. Therefore, multidimensional CBCA(CO)NH (15) and HNCACB (16) experiments have emerged as the most commonly used pair of NMR experiments for the sequential resonance assignments of uniformly ^{13}C, ^{15}N labeled proteins. However, in HNCACB spectra, both intraresidue and interresidue correlations are present, since the one-bond $^1J_{NCA}$ and the two-bond $^2J_{NCA}$ couplings are of similar magnitude. This frequently makes it difficult to distinguish intra- from interresidue connectivities. Schemes for eliminating the intraresidue correlations by suppressing coherence transfer via the one bond $^1J_{NCA}$ couplings have been reported to alleviate such ambiguities (*17, 18*). In a complementary approach, it may be equally desirable to eliminate interresidue correlations arising from two-bond $^2J_{NCA}$ couplings in HNCACB spectra, resulting in improved resolution of intraresidue HNCACB correlation spectra.

[1] Author to whom correspondence should be addressed. E-mail: gronenborn@nih.gov.

1090-7807/02 $35.00

Here, we present a novel pulse sequence building block aimed at retaining only the intraresidue HNCACB correlations arising from one-bond $^1J_{NCA}$ couplings. By incorporating this pulse scheme, a HN(COCA)CACB experiment can be developed that yields information about intraresidue correlations between amide proton and nitrogen chemical shifts and α- and β-carbon chemical shifts.

In a second type of experiment, correlations between amide proton and nitrogen chemical shifts and α-carbon and -proton chemical shifts between neighboring amino acids are exploited. Based on the high sensitivity of magnetization transfer from α-carbon to α-proton, it appeared appealing to also use the α-proton instead of the β-carbon for the sequential resonance assignment. In this case it is mandatory to achieve excitation of α-protons without exciting the water and amino-proton resonances. The pulse scheme described here for the HN(CO)CAHA and HN(COCA)CAHA experiments provides this feature.

All four experiments are presented as 2D versions. We demonstrate the applicability of these four pulse schemes for the small protein GB1 (*19*). As is easily appreciated, these experiments retain the same resolution as 2D ^{1}H–^{15}N HSQC spectra (*20, 21*) and thereby can be employed as an efficient and fast means for sequential resonance assignments of small to medium-sized proteins.

HN(CO)CACB AND HN(COCA)CACB EXPERIMENTS

The 2D HN(CO)CACB experiment is a simple modification of the 3D HN(CO)CACB experiment. As shown in Fig. 1A, the pulse sequence consists of several common building blocks, including a forward and backward INEPT transfer step (*22*) H $\leftrightarrow$ N $\leftrightarrow$ CO $\leftrightarrow$ CA at the beginning and the end. After the initial INEPT transfer step, the magnetization $8CA_xCO_zN_zH_z$ is prepared, denoted as CA_xN_z for simplicity. An incomplete INEPT transfer step to β-carbon with the delay Δ_1 set by $8\Delta_1 J_{CC} = 1$ and a 54°-pulse on ^{15}N converts CA_xN_z into four terms of magnetization: CA_xN_z, $-2CB_xCA_zN_z$, CA_xN_x and $-2CB_xCA_zN_x$, which can be obtained from a simple analysis in the product operator formalism (*23*). After the evolution period, all four terms of magnetization are transformed back into detectable proton transverse magnetization by the corresponding backward magnetization transfer steps. Since ^{15}N evolution is amplitude modulated, these four terms of magnetization yield six kinds of cross peaks in the 2D spectrum, that is, (ω_{CA}, ω_H), (ω_{CB}, ω_H), $(\omega_{CA} + \omega_N, \omega_H)$, $(\omega_{CA} - \omega_N, \omega_H)$, $(\omega_{CB} + \omega_N, \omega_H)$, $(\omega_{CB} - \omega_N, \omega_H)$.

The general strategy to manipulate these six kinds of cross peaks in a 2D spectrum is depicted in Fig. 2A, which presents the experimental spectrum recorded using the pulse sequences

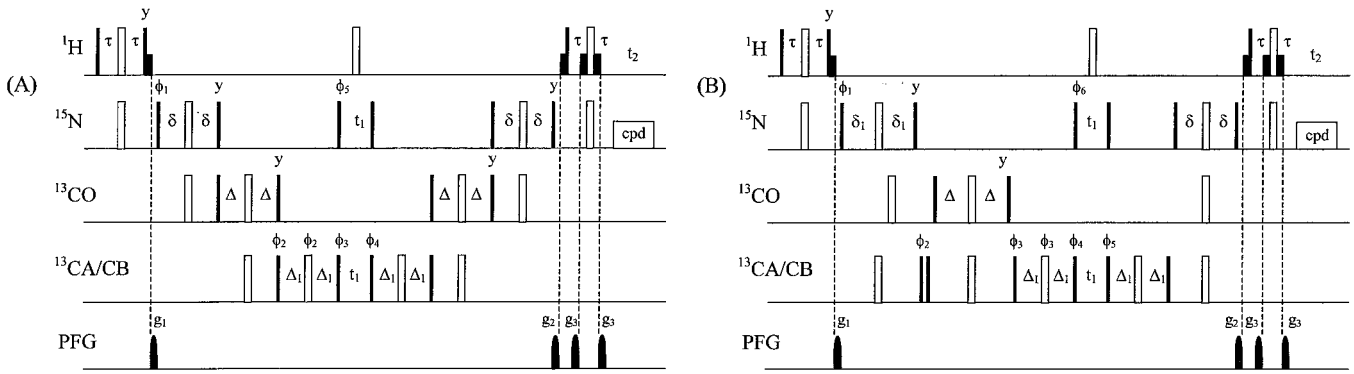

FIG. 1. Pulse sequences for the 2D HN(CO)CACB and the 2D HN(COCA) CACB experiments. Narrow (filled) and wide (open) bars represent 90° and 180° pulses with phase x, respectively, unless indicated otherwise. The two filled bars in ^{15}N that sandwich the evolution period represent 54° pulses. Proton pulses are on resonance at the water peak position. Proton 90° soft pulses of 1-ms duration are used for water flip-back and Watergate, and these are indicated by short filled bars. The carrier frequency for ^{13}CO is set at 177 ppm. The 90° and 180° pulses for ^{13}CO are applied at the power levels of $\Delta\omega_0/(15)^{1/2}$ and $\Delta\omega_0/(3)^{1/2}$, respectively, resulting in zero excitation at 56 ppm, with $\Delta\omega_0$ the difference in Hz between the center of the $^{13}C\alpha$ chemical shift range (56 ppm) and the ^{13}CO carrier frequency (177 ppm) (*27*). The carrier frequency for $^{13}C\alpha/^{13}C\beta$ is positioned at 43 ppm. The narrow (filled) and wide (open) bars sandwiching the delays Δ_1 and t_1 for $^{13}C\alpha/^{13}C\beta$ are 270° and 540° pulses, respectively, applied at the power level of $3\Delta\omega_0/(7)^{1/2}$, resulting in zero excitation at 177 ppm, with $\Delta\omega_0$ the difference in Hz between the $^{13}C\alpha/^{13}C\beta$ and the ^{13}CO carrier frequencies (*27*). The remaining pulses for $^{13}C\alpha/^{13}C\beta$ are 90° and 180° pulses applied at the power levels of $\Delta\omega_0/(15)^{1/2}$ and $\Delta\omega_0/(3)^{1/2}$, respectively, resulting in zero excitation at 177 ppm, with $\Delta\omega_0$ the difference in Hz between the $^{13}C\alpha/^{13}C\beta$ and the ^{13}CO carrier frequencies (*27*). The 90° pulse for ^{13}CO at phase y is additionally phase-shifted to account for the effect of the 180° pulse applied to $^{13}C\alpha/^{13}C\beta$, by $360(\Delta\omega_0\tau_{180})$ degrees with $\Delta\omega_0$ representing the difference in Hz between the $^{13}C\alpha/^{13}C\beta$ and the ^{13}CO carrier frequencies and τ_{180} is the width of the 180° pulse in seconds. The PFG pulses g_1, g_2, and g_3 are sine shaped with maximal 20 G/cm, exhibiting pulse lengths of 3, 1.5, and 0.6 ms, respectively. ^{15}N decoupling during t_2 was achieved using WALTZ-16 sequence (*28*). In (A), the interpulse delays are $\tau = 2.25$ ms, $\delta = 17.5$ ms, $\Delta = 5$ ms, and $\Delta_1 = 4$ ms; the phase cycles are as follows: $\phi_1 = x, -x$; $\phi_2 = x, x, -x, -x$; $\phi_3 = 4(y), 4(-y)$; $\phi_4 = 4(y), 8(-y), 4(y)$; $\phi_5 = x$; and $\phi_{Rec} = x, -x, -x, x$; the phases ϕ_2 and ϕ_3 are incremented by 90° (*29*) to achieve quadrature detection in the ω_1 dimension and the phase ϕ_5 is incremented by 120° time-proportionally to create an artificial resonance offset for ^{15}N. In (B), the interpulse delays are $\tau = 2.25$ ms, $\delta_1 = 25$ ms, $\delta = 12.5$ ms, $\Delta = 5$ ms, and $\Delta_1 = 4$ ms; the phase cycles are as follows: $\phi_1 = x, -x$; $\phi_2 = x, x, -x, -x$; $\phi_3 = 4(x), 4(-x)$; $\phi_4 = 4(y), 8(-y), 4(y)$; $\phi_5 = 8(y), 16(-y), 8(y)$; $\phi_6 = x$; and $\phi_{Rec} = x, -x, x, -x, -x, x, -x, x$; the phases ϕ_3 and ϕ_4 are incremented by 90° (*29*) to achieve quadruture detection in the ω_1 dimension and the phase ϕ_6 is incremented by 120° time-proportionally to create an artificial resonance offset for ^{15}N.

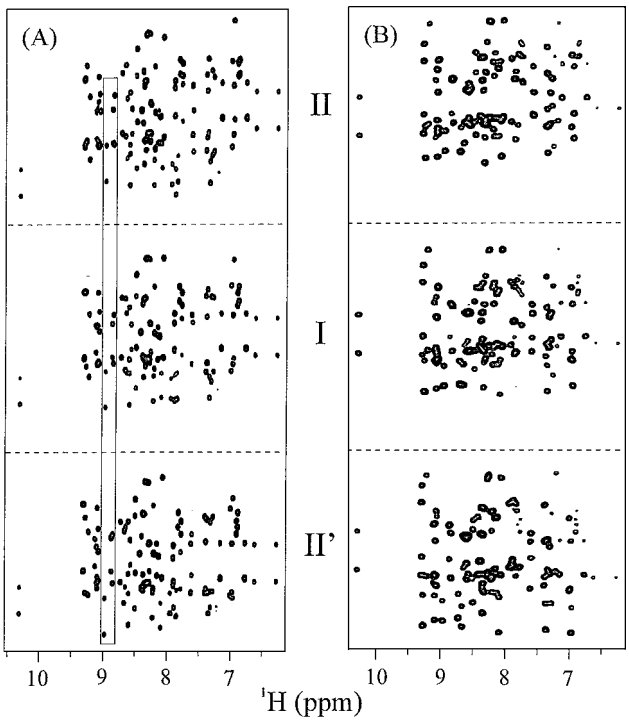

FIG. 2. Experimental 2D HN(CO)CACB (A) and 2D HN(COCA)CACB (B) spectra recorded on a 1-mM sample of uniformly ^{13}C, ^{15}N labeled protein GB1 in 95% H_2O/5% D_2O at pH 5.5 employing the pulse scheme presented in Figs. 1A and 1B, respectively. The 2D HN(CO)CACB spectrum was recorded on a Bruker DMX 500 spectrometer using the following parameters: spectral width, $SW_1 \times SW_2 = 31250 \times 7507.507$ Hz; time domain data set, $TD_1 \times TD_2 = 320 \times 1024$; ns = 64; window functions in both dimensions are squared sine bell; zero filling to 1024×1024; recycle delay is 1 s. The total experimental time was 7.5 h. The 2D HN(COCA)CACB spectrum was recorded on a Bruker DMX 600 spectrometer using the following parameters: spectral width, $SW_1 \times SW_2 = 40000 \times 7788.162$ Hz; time domain data set, $TD_1 \times TD_2 = 320 \times 512$; ns = 160; window functions in both dimensions are squared sine bell; zero filling to 1024×1024; recycle delay is 1 s. The total experimental time was 17.5 h. Data were processed by using nmrPipe and nmrDraw software (*30*).

of Fig. 1A. First, the spectral width acquired in the ω_1 dimension, SW_1, is set to be equal or larger than $2SW_N + 3SW_{CA} + 3SW_{CB}$, with SW_N, SW_{CA}, and SW_{CB} representing the spectral widths for ^{15}N, $^{13}C^{\alpha}$, and $^{13}C^{\beta}$ resonances. Second, TPPI (*24, 25*) is used to create an artificial large resonance offset in ^{15}N, dividing the 2D spectrum into three distinct regions, labeled I, II, and II′ in Fig. 2A. Region I contains the cross peaks (ω_{CA}, ω_H) and (ω_{CB}, ω_H). Except for Ser and Thr (*26*), $^{13}C^{\alpha}$ and $^{13}C^{\beta}$ resonances are hardly overlapping and disperse into different regions. Since, however, the cross peaks (ω_{CA}, ω_H) and (ω_{CB}, ω_H) are of opposite signs, it is easy to distinguish between them. In region II (upper 1/3), cross peaks ($\omega_{CA} - \omega_N$, ω_H) and ($\omega_{CB} - \omega_N$, ω_H) are found, while in region II′ (lower 1/3) the cross peaks ($\omega_{CA} + \omega_N$, ω_H) and ($\omega_{CB} + \omega_N$, ω_H) are present. Individual components of cross-peak pairs reside in regions II and II′ centered around a single cross peak in region I. The distance between each peak in a pair provides the ^{15}N frequency ω_N. In this manner, all four chemical shifts for $H^N(i)$, $N(i)$, $C^{\alpha}(i-1)$, and $C^{\beta}(i-1)$ can be obtained from a single 2D spectrum. This is most easily appreciated from the expanded region of the HN(CO)CACB spectrum displayed in Fig. 3. Cross peaks for three sequential amino acid dipeptide stretches of the GB1 sequence comprising T18/T17, D36/N35, and N8/L7 are shown and labeled with the pertinent parameters. The chemical shift values for $H^N(i)$, $C^{\alpha}(i-1)$, and $C^{\beta}(i-1)$, can be read directly from the cross peaks in region I and that of $^{15}N(i)$ can be calculated from the splitting ($\Delta_{II,II'}$) between each of the two peaks of the pair, where $\Delta_{II,II'} = 2\omega_{N(i)} + 2SW_1/n$, with SW_1 the spectral width in the ω_1 dimension and $n = 360/\Delta\phi_N$ and $\Delta\phi_N$ representing the phase incrementation in TPPI (*24, 25*). After $\omega_{N(i)}$ is obtained, the chemical shift value $\delta_{N(i)}$ of $^{15}N(i)$ is given by $\delta_{N(i)} = \omega_{N(i)}/\omega_{0N} + \delta_{0N}$, where ω_{0N} is the spectrometer frequency in ^{15}N and δ_{0N} is the chemical shift value at the position of the carrier frequency.

In order to extract a set of four intraresidue chemical shifts for $H^N(i)$, $N(i)$, $C^{\alpha}(i)$, and $C^{\beta}(i)$ in a single 2D spectrum, a 2D HN(COCA)CACB experiment was developed. This set of chemical shifts allows one to complete the sequential resonance assignment. The implementation of the 2D HN(COCA)CACB experiment is more complex and demanding. In any heteronuclear experiment that utilizes magnetization transfer between $^{13}C^{\alpha}$ and ^{15}N via J_{NCA}, discrimination between the direct one-bond $N(i) \leftrightarrow CA(i)$ and the two-bond $N(i) \leftrightarrow CA(i-1)$ magnetization transfer is impossible, since the one-bond and two-bond J_{NCA} couplings are of similar magnitude. In the classical HN(CO)CACB experiment, this kind of problem is solved

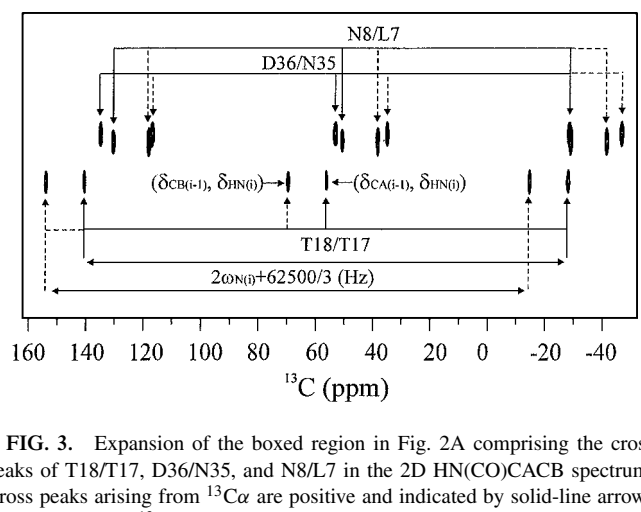

FIG. 3. Expansion of the boxed region in Fig. 2A comprising the cross peaks of T18/T17, D36/N35, and N8/L7 in the 2D HN(CO)CACB spectrum. Cross peaks arising from $^{13}C\alpha$ are positive and indicated by solid-line arrows while those from $^{13}C\beta$ are negative and indicated by dashed-line arrows. The chemical shift values of $\delta_{HN(i)}$, $\delta_{CA(i-1)}$, and $\delta_{CB(i-1)}$ are extracted directly from the cross-peak positions in region I. The distance $\Delta_{II,II'}$ for a peak pair in regions II and II′ is given by $\Delta_{II,II'} = 2\omega_{N(i)} + 2SW_1/n$, where SW_1 is the spectral width in the ω_1 dimension and $n = 360/\Delta\phi_N$, with $\Delta\phi_N$ representing the phase incremention in TPPI. From this difference $\omega_{N(i)}$ is obtained and the chemical shift value $\delta_{N(i)}$ for $^{15}N(i)$ is calculated by $\delta_{N(i)} = \omega_{N(i)}/\omega_{0N} + \delta_{0N}$, with ω_{0N} the spectrometer frequency in ^{15}N and δ_{0N} is the chemical shift value at the carrier frequency position.

by relaying via ^{13}CO for which solely one-bond couplings are significant and therefore only sequential assignments are observed. In the present case we want to only observe correlations caused by the direct one-bond $N(i) \leftrightarrow CA(i)$ transfer and eliminate any complications arising from the two-bond $N(i) \leftrightarrow CA(i-1)$ transfer for simplification of the spectrum. The pulse sequence devised for the current 2D HN(COCA)CACB experiment utilizes three transfers, exploiting the one-bond $^1J_{NCA}$, $^1J_{NCO}$ and two-bond $^2J_{NCA}$ couplings to create 4-spin order $N(i)_zCO(i-1)_zCA(i-1)_zCA(i)_z$. The first two 90° pulses on ^{13}CA/CB are applied as filters to select this 4-spin order. The subsequent $CO(i-1) \leftrightarrow CA(i-1)$ INEPT transfer step transforms $N(i)_zCO(i-1)_zCA(i-1)_zCA(i)_z$ magnetization into $N(i)_zCO(i-1)_zCA(i)_z$ magnetization. Since the magnetization $N(i)_zCO(i-1)_zCA(i)_z$ is prepared via one-bond $^1J_{NCO}$ and two-bond $^2J_{NCA}$ couplings to $CO(i-1)_zCA(i-1)_z$, this experiment is equivalent to a 2D HN(COCA)CACB experiment. As in the 2D HN(CO)CACB experiment, an incomplete INEPT transfer step to $^{13}C^\beta$ with the delay Δ_1 set to $8\Delta_1 J_{CC} = 1$ and a 54°-pulse on ^{15}N are used to convert $N(i)_zCO(i-1)_z$ $CA(i)_z$ magnetization into four discrete terms of magnetization: $CA(i)_xN(i)_zCO(i-1)_z$, $-2CB(i)_xCA(i)_zN(i)_zCO(i-1)_z$, $CA(i)_xN_x(i)CO(i-1)_z$, $-2CB(i)_xCA(i)_zN(i)_xCO(i-1)_z$. After the evolution period, these are transformed back into $N(i)_zCO(i-1)_zCA(i)_z$ magnetization which subsequently is converted back to $N(i)$ by one-bond $^1J_{NCA}$, $^1J_{NCO}$ and two-bond $^2J_{NCA}$ couplings and finally into detectable proton transverse magnetization in the detection period. Six kinds of cross peaks, (ω_{CA}, ω_H), (ω_{CB}, ω_H), $(\omega_{CA}+\omega_N, \omega_H)$, $(\omega_{CA}-\omega_N, \omega_H)$, $(\omega_{CB}+\omega_N, \omega_H)$, and $(\omega_{CB}-\omega_N, \omega_H)$, are present in the resulting 2D spectrum. The equivalent strategy as described above for the 2D HN(CO)CACB spectrum is used to identify cross peaks in the different regions of the single 2D HN(COCA)CACB spectrum.

The pulse sequence for the HN(COCA)CACB experiment is outlined in Fig. 1B and the 2D spectrum recorded with this sequence is shown in Fig. 2B.

HN(CO)CAHA AND HN(COCA)CAHA EXPERIMENTS

In order to extend the assignments to H^α protons, or, alternatively, to provide backbone assignments only, without extending into the side chain $^{13}C^\beta$ resonances, two additional experiments were developed. As depicted in Fig. 4, the pulse sequences for the 2D HN(CO)CAHA and HN(COCA)CAHA experiments are modifications of those used for 2D HN(CO)CACB and HN(COCA)CACB experiments. Instead of the incomplete INEPT step from the $^{13}C^\alpha$ to the attached $^{13}C^\beta$ in the HN(CO)CACB and HN(COCA)CACB experiments, a complete INEPT transfer is carried out for the attached H^α proton in the HN(CO)CAHA and HN(COCA)CAHA experiments. Although the magnetization transfer from C^α to H^α is very efficient, it is rarely implemented in NMR experiments used for protein structure determinations. The mainbreak reason for this may be the

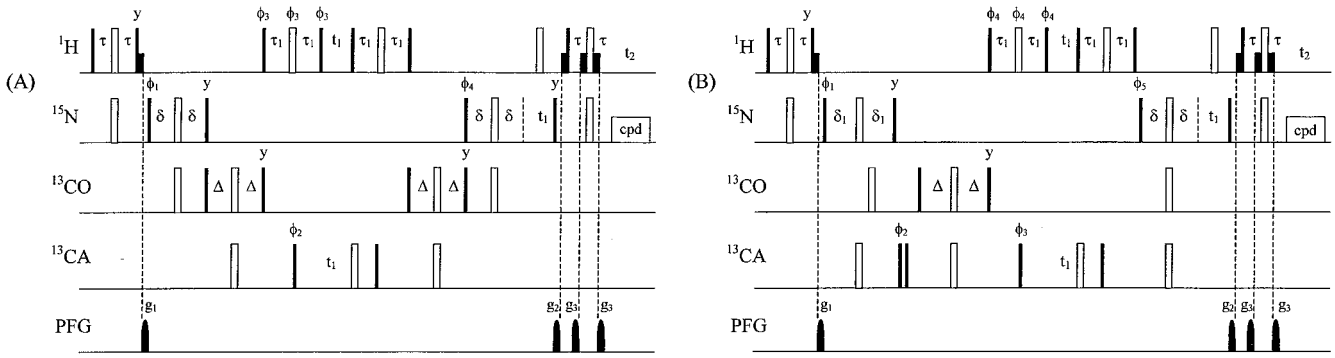

FIG. 4. Pulse sequences for the 2D HN(CO)CAHA and 2D HN(COCA) CAHA experiments. Narrow (filled) and wide (open) bars represent 90° and 180° pulses with phase x, respectively, unless indicated otherwise. The proton pulses are on resonance at the water peak position. Proton 90° soft pulses of 1-ms duration are used for water flip-back and Watergate, and these are indicated by short filled bars. The carrier frequency for ^{13}CO is set at 177 ppm. The 90° and 180° pulses applied for ^{13}CO are applied at power levels of $\Delta\omega_0/(15)^{1/2}$ and $\Delta\omega_0/(3)^{1/2}$, respectively, resulting in zero excitation at 56 ppm, with $\Delta\omega_0$ the difference in Hz between the $^{13}C\alpha$ carrier frequency (56 ppm) and ^{13}CO carrier frequency (177 ppm) (*27*). The narrow (filled) and wide (open) bars for $^{13}C\alpha$ are 270° and 540° pulses, respectively, applied at the power level of $3\Delta\omega_0/(7)^{1/2}$, resulting in zero excitation at 177 ppm, with $\Delta\omega_0$ the difference in Hz between the $^{13}C\alpha$ and the ^{13}CO carrier frequencies (*27*). The 90° pulse for ^{13}CO at phase y is additionally phase-shifted to account for the effect of the 180° pulse applied to $^{13}C\alpha$, by $360(\Delta\omega_0\tau_{180})$ degrees with $\Delta\omega_0$ representing the difference in Hz between the $^{13}C\alpha$ and the ^{13}CO carrier frequencies and τ_{180} is the width of the 180° pulse in seconds. The PFG pulses g_1, g_2, and g_3 are sine shaped with maximal 20 G/cm, exhibiting pulse lengths of 3, 1.5, and 0.6 ms, respectively. The HA magnetization is flipped by 90° using the sequence 90°–τ_1–180°–τ_1–90°, instead of a single 90° pulse, since this does not perturb the water magnetization. Solvent suppression by water flip-back and/or Watergate is therefore not affected. ^{15}N decoupling during t_2 was achieved using WALTZ-16 sequence (*28*). In (A), the interpulse delays are $\tau = 2.25$ ms, $\delta = 17.5$ ms, $\Delta = 5$ ms, $\tau_1 = 3.8$ ms, and $\Delta_1 = 4$ ms; the phase cycles are as follows: $\phi_1 = x, -x$; $\phi_2 = x, x, -x, -x$; $\phi_3 = 4(x), 4(-x)$; $\phi_4 = x$; and $\phi_{Rec} = x, -x, -x, x, -x, x, x, -x$; the phase ϕ_2 is incremented by 90° (*29*) to achieve quadrature detection in the ω_1 dimension and the phases ϕ_3 and ϕ_4 are incremented by 45° and 90° time-proportionally to create artificial resonance offsets in ^{1}H and ^{15}N, respectively. In (B), the interpulse delays are $\tau = 2.25$ ms, $\delta_1 = 25$ ms, $\delta = 12.5$ ms, $\Delta = 5$ ms, $\tau_1 = 3.4$ ms, and $\Delta_1 = 4$ ms; the phase cycles are as follows: $\phi_1 = x, -x$; $\phi_2 = x, x, -x, -x$; $\phi_3 = 4(x), 4(-x)$; $\phi_4 = 8(x), 8(-x)$; $\phi_5 = x$; and $\phi_{Rec} = 2(x, -x), 4(-x, x), 2(x, -x)$; the phase ϕ_3 is incremented by 90° (*29*) to achieve quadrature detection in the ω_1 dimension and the phases ϕ_4 and ϕ_5 are incremented by 45° and 90° time-proportionally to create artificial resonance offsets in ^{1}H and ^{15}N, respectively.

resonance overlap between the water and the α-proton resonances, making it very difficult not to disturb the water magnetization when manipulating that of α-protons. Even if band-selective pulses are employed, the disturbance of the water signal is unavoidable, so that the water suppression fails. Here we use a 90°–τ_1–180°–τ_1–90° sequence, instead of a single 90° pulse, to excite H^α magnetization. In this manner, the water and amino-proton resonances are not perturbed. Therefore, no interference of amino protons in the evolution periods is observed and solvent suppression using water flip-back (*31*) or Watergate (*32*) is not affected. Thus formally, the current HN(CO)CAHA and HN(COCA)CAHA experiments achieve magnetization transfer from C^α to H^α via heteronuclear one-bond scalar couplings.

The general strategy for implementing this pair of experiments is different from that described in the preceding section. In the evolution period, only a single magnetization is retained, namely $N_xCA_xHA_x$, with the operator factor of the magnetizations H^N and CO omitted for simplicity, which can be obtained from a simple analysis in the product operator formalism (*23*). Since any one of the three frequencies ^{15}N, $^{13}C^\alpha$, and $^1H^\alpha$ can be selected for quadrature detection, with the remaining two frequencies used for splitting the peaks, three choices exist for setting up these experiments. The resolutions of the resulting spectra in these three settings are slightly different. In the present study, quadrature detection via States (*29*) is used for $^{13}C^\alpha$. The evolution of $^{13}C^\alpha$ magnetization can be expressed by exponential $\mathrm{EXP}(i\omega_{CA}t_1)$ and the evolutions of ^{15}N and $^1H^\alpha$ are the cosine amplitude modulations. Thus, altogether, the evolution of magnetization $N_xCA_xHA_x$ during the evolution period can be expressed as $\mathrm{COS}(i\omega_{HA}t_1)\,\mathrm{COS}(i\omega_N t_1)\,\mathrm{EXP}(i\omega_{CA}t_1)$. This kind of t_1-modulation results in four groups of cross peaks, namely $(\omega_{CA}+\omega_N+\omega_{HA},\ \omega_H)$, $(\omega_{CA}-\omega_N+\omega_{HA},\ \omega_H)$, $(\omega_{CA}+\omega_N-\omega_{HA},\ \omega_H)$, and $(\omega_{CA}-\omega_N-\omega_{HA},\ \omega_H)$. Essentially as described above for the HN(CO)CACB and HN(COCA)CACB experiments, the spectral width in the ω_1 dimension, SW_1, is equal or larger than $4SW_N+4SW_{CA}+4SW_{HA}$, with SW_N, SW_{CA}, and SW_{HA} representing the spectral widths for ^{15}N, $^{13}C^\alpha$, and $^1H^\alpha$ resonances. TPPI (*24, 25*) is used to generate artificial large resonance offsets for ^{15}N and $^1H^\alpha$ such that the four groups of cross peaks are located in four distinct regions, labeled I, I′, II, and II′ in Fig. 5. Using the phase incrementation described in the figure caption of Fig. 4, cross peaks $(\omega_{CA}-\omega_N+\omega_{HA},\ \omega_H)$ and $(\omega_{CA}+\omega_N-\omega_{HA},\ \omega_H)$ are located in the I and I′ regions, respectively. Cross peaks $(\omega_{CA}-\omega_N-\omega_{HA},\ \omega_H)$ and $(\omega_{CA}+\omega_N+\omega_{HA},\ \omega_H)$ are located in regions II and II′, respectively.

The experimental spectra recorded using the pulse sequences depicted in Fig. 4 are displayed in Fig. 5. Sequential resonance assignments of H^N, N, C^α, and H^α can be obtained easily from these two spectra. Note the excellent resolution present in the spectra.

Figure 6 illustrates a small region extracted from the 2D HN(CO)CAHA spectrum expanding the area around the cross peaks of K28/E27 and T49/A48. Again, interpretation of the

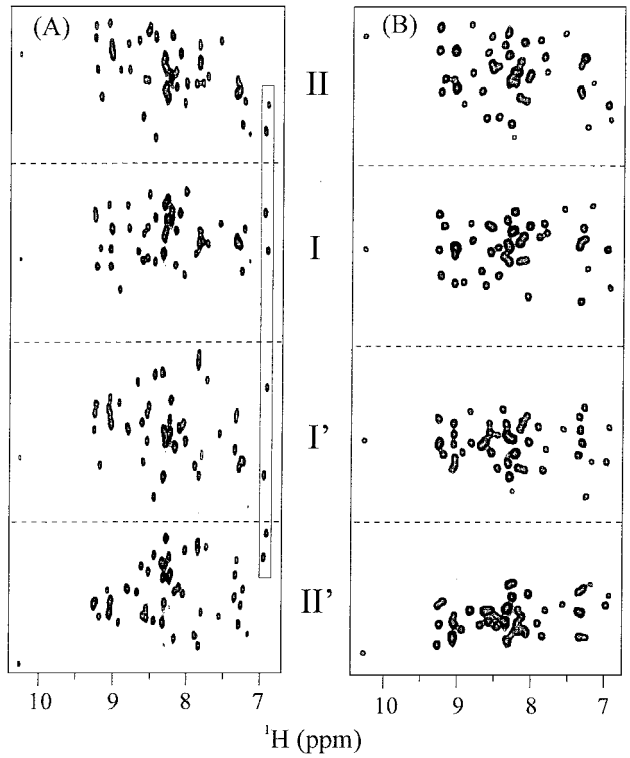

FIG. 5. Experimental 2D HN(CO)CAHA (A) and 2D HN(COCA)CAHA (B) spectra recorded on a 1-mM sample of uniformly ^{13}C, ^{15}N labeled protein GB1 in 95% H_2O/5% D_2O at pH 5.5, employing the pulse schemes presented in Figs. 4A and 4B, respectively. The 2D HN(CO)CAHA spectrum was recorded on a Bruker DMX 500 spectrometer using the following parameters: spectral width, $SW_1 \times SW_2 = 16000 \times 7507.507$ Hz; time domain data set, $TD_1 \times TD_2 = 320 \times 1024$; ns = 64; window functions in both dimensions are squared sine bell; zero filling to 1024×1024; recycle delay is 1 s. The total experimental time was 7.5 h. The 2D HN(COCA)CAHA spectrum was recorded on a Bruker DMX 600 spectrometer using the following parameters: spectral width, $SW_1 \times SW_2 = 25000 \times 7788.162$ Hz; time domain data set, $TD_1 \times TD_2 = 256 \times 512$; ns = 64; window functions in both dimensions are squared sine bell; zero filling to 1024×1024; recycle delay is 1 s. The total experimental time was less than 6 h. Data were processed by using nmrPipe and nmrDraw software (*30*).

spectra is straightforward. The chemical shift values of $\delta_{HN(i)}$ and $\delta_{CA(i-1)}$ can be directly read off at the middle of the cross-peak pairs in the regions I and II. The distances $\Delta_{I,I'}$ and $\Delta_{II,II'}$ within the peak pair in regions I and I′ and in regions II and II′ can be expressed by $\Delta_{I,I'} = 2(\omega_{N(i)} + SW_1/n) - 2(\omega_{HA(i-1)} + SW_1/m)$ and $\Delta_{II,II'} = 2(\omega_{N(i)} + SW_1/n) + 2(\omega_{HA(i-1)} + SW_1/m)$, respectively, where SW_1 is the spectral width in the ω_1 dimension, $n = 360/\Delta\phi_N$ with $\Delta\phi_N$ representing the phase incrementation in TPPI (*24, 25*) for ^{15}N, and $m = 360/\Delta\phi_{HA}$ with $\Delta\phi_{HA}$ representing the phase incrementation TPPI (*24, 25*) process for the α-protons. After extraction of $\omega_{N(i)}$ and $\omega_{HA(i-1)}$, the chemical shift value $\delta_{N(i)}$ is calculated by $\delta_{N(i)} = \omega_{N(i)}/\omega_{0N} + \delta_{0N}$, with ω_{0H} the spectrometer frequency for ^{15}N and δ_{0N} the chemical shift value at the carrier frequency position. The chemical shift value $\delta_{HA(i-1)}$ is calculated using $\delta_{HA(i-1)} = \omega_{HA(i-1)}/\omega_{0H} + \delta_{0H}$,

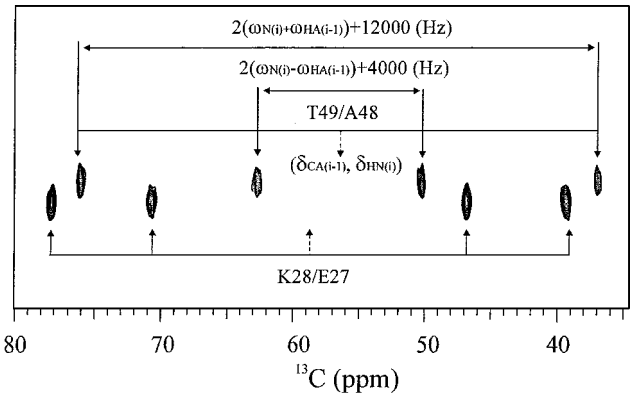

FIG. 6. Expansion of the boxed region in Fig. 5A comprising the cross peaks of K28/E27 and T49/A48 in 2D HN(CO)CAHA. The centers for the cross-peak pairs in regions I, I′ and regions II, II′ coincide and the position is indicated by dashed-line arrow. The chemical shift values of $\delta_{\mathrm{HN}(i)}$ and $\delta_{\mathrm{CA}(i-1)}$ can be read directly from the common center position of the cross-peak pairs in the regions I, I′ and II, II′. The distance $\Delta_{\mathrm{I,I'}}$ within the peak pair in regions I and I′ can be expressed by $\Delta_{\mathrm{I,I'}} = 2(\omega_{\mathrm{N}(i)} + \mathrm{SW}_1/n) - 2(\omega_{\mathrm{HA}(i-1)} + \mathrm{SW}_1/m)$, while the distance $\Delta_{\mathrm{II,II'}}$ within the peak pair in regions II and II′ can be expressed by $\Delta_{\mathrm{II,II'}} = 2(\omega_{\mathrm{N}(i)} + \mathrm{SW}_1/n) + 2(\omega_{\mathrm{HA}(i-1)} + \mathrm{SW}_1/m)$, where SW_1 is the spectral width in the ω_1 dimension, $n = 360/\Delta\phi_{\mathrm{N}}$ with $\Delta\phi_{\mathrm{N}}$ representing the phase incrementation in TPPI for ^{15}N, and $m = 360/\Delta\phi_{\mathrm{HA}}$ with $\Delta\phi_{\mathrm{HA}}$ representing the phase incrementation in TPPI for the α-protons. From these differences, $\omega_{\mathrm{N}(i)}$ and $\omega_{\mathrm{HA}(i-1)}$ are obtained, and the chemical shift value of $\delta_{\mathrm{N}(i)}$ is calculated by $\delta_{\mathrm{N}(i)} = \omega_{\mathrm{N}(i)}/\omega_{0\mathrm{N}} + \delta_{0\mathrm{N}}$, with $\omega_{0\mathrm{N}}$ the spectrometer frequency in ^{15}N and $\delta_{0\mathrm{N}}$ the chemical shift value at the carrier frequency position. The chemical shift value of $\delta_{\mathrm{HA}(i-1)}$ is calculated by $\delta_{\mathrm{HA}(i-1)} = \omega_{\mathrm{HA}(i-1)}/\omega_{0\mathrm{H}} + \delta_{0\mathrm{H}}$, with $\omega_{0\mathrm{H}}$ the spectrometer frequency for protons and $\delta_{0\mathrm{H}}$ the chemical shift value at the carrier frequency position.

with $\omega_{0\mathrm{H}}$ the spectrometer frequency for protons and $\delta_{0\mathrm{H}}$ the chemical shift value at the position of the carrier frequency position.

DISCUSSION

In contrast to the traditional 2D experiments, the 2D experiments proposed here contain two or three evolution processes combined into a common dimension. Evolution of magnetization for the individual processes possesses contributions from the phase acquired in t_1 by the resonance offset and from the phase incremented in the TPPI process (*24, 25*). One technical difficulty encountered in setting up these 2D experiments is to ensure good phase properties of the acquired spectra. To allow for easy phasing of the spectra, all the initial times in the different evolution processes have to be set to be proportional and the initial phase increments for TPPI (*24, 25*) need to be proportional to the initial t_1 value. As a special case, 180° pulses can be used to compensate for the initial t_1 value such that all the evolution processes begin at time zero. In this case, no initial phase increments are necessary for the TPPI processes (*24, 25*).

In order to further improve the digital resolution in the ω_1 dimension, linear prediction can be employed (*33*). As a matter of fact, doubling the data points by linear prediction before zero filling for the spectra displayed in Figs. 2 and 5 results in substantial increases in the resolution (data not shown). For practical applications, we therefore strongly suggest such data processing prior to 2D Fourier transformation.

Although the current experiments are performed on the small protein GB1, our experimental scheme applies equally well to medium-sized proteins. The resolution of these 2D experiments is critically determined by the resolution of normal 2D ^{15}N–^{1}H HSQC or 2D H(NCO)CA spectra, and, barring severe overlap in the latter, the presented schemes will work satisfactorily. These spectra will exhibit the least overlap since the amide resonances are generally well dispersed and, barring severe overlap, the presented schemes will work satisfactorily. Even in cases of amide degeneracy, it will be possible to arrive at the assignment since simultaneous degeneracy in $^{13}C^{\alpha}$ is extremely unlikely. Furthermore, if good resolution of the 2D TROSY (*34*) spectrum is observed, the current experiments can be extended into their TROSY versions. This will be very useful for very large, oligomeric proteins.

The sensitivity of 2D HN(CO)CACB, HN(COCA)CACB is $(2)^{1/2}/3$ times that of their 3D counterparts and the sensitivity of HN(CO)CAHA and HN(COCA)CAHA is 1/2 of their 4D counterparts (*11*). In cases where sample concentration is not a limiting factor, improvement of digital resolution in multidimensional experiments is frequently the main reason for long experiment times. The current 2D experiments can be used as efficient and sensitive alternatives.

An immediate practical application of such 2D spectra with three or four chemical shift correlations is their use in NMR screening approaches (*35–37*), for which 3D or 4D experiments are ill suited.

In summary, a suite of novel triple resonance 2D experiments are proposed as a fast and efficient means for sequential resonance assignments of proteins. Here we describe four of these, namely 2D HN(CO)CACB, HN(COCA)CACB, HN(CO)CAHA, and HN(COCA)CAHA experiments. The strategy employed for implementing these kinds of 2D versions is easily extended to other types of 3D and 4D experiments, commonly used for protein structure determinations. In addition, we are currently extending the above strategy to experiments aimed at accurate measurements of coupling constants. In particular, a set of high-resolution 2D experiments for the determination of one-bond H–N, N–CO, CO–CA, and CA–HA ($J + D$) couplings is under development. These new types of 2D experiments should become extremely useful in NMR structural studies of small to medium-sized proteins in solutions, especially if automated procedures are applied in structural genomics projects. Peak lists derived from these 2D experiments should be easily extracted given the high resolution of the spectra with tight match tolerances for chemical shifts. Such peak lists may be used in programs for automated sequence specific assignments, making structure determination of proteins by NMR a much easier and faster process in the near future.

ACKNOWLEDGMENT

This work was supported in part by the Intramural AIDS Targeted Antiviral Program of the Office of the Director of the National Institutes of Health to AMG.

REFERENCES

1. G. M. Clore and A. M. Gronenborn, *Science* **252,** 1390–1399 (1991).
2. A. Bax and S. Grzesiek, *Acc. Chem. Res.* **26,** 131–138 (1993).
3. D. S. Garrett, R. Powers, A. M. Gronenborn, and G. M. Clore, *J. Magn. Reson.* **95,** 214–220 (1991).
4. B. A. Johnson and R. A. Blevins, *J. Biomol. NMR* **4,** 603–614 (1994).
5. R. Koradi, M. Billeter, M. Engeli, P. Guntert, and K. Wüthrich, *J. Magn. Reson.* **135,** 288–297 (1998).
6. T. Szyperski, G. Wider, J. H. Bushweller, and K. Wüthrich, *J. Biomol. NMR* **3,** 127–132 (1993).
7. T. Szyperski, G. Wider, J. H. Bushweller, and K. Wüthrich, *J. Am. Chem. Soc.* **115,** 9307–9308 (1993).
8. B. Brutscher, J. P. Simorre, M. S. Caffrey, and D. Marion, *J. Magn. Reson. Ser. B* **105,** 77–82 (1994).
9. J. P. Simorre, B. Brutscher, M. S. Caffrey, and D. Marion, *J. Biomol. NMR* **4,** 325–334 (1994).
10. F. Löhr and H. Rüterjans, *J. Biomol. NMR* **6,** 189–197 (1995).
11. B. Brutscher, F. Cordier, J. P. Simorre, M. S. Caffrey, and D. Marion, *J. Biomol. NMR* **5,** 202–206 (1995).
12. T. Szyperski, D. Braun, C. Bartels, and K. Wüthrich, *J. Magn. Reson. Ser. B* **108,** 197–203 (1995).
13. T. Szyperski, B. Banecki, D. Braun, and R. W. Glaser, *J. Biomol. NMR* **11,** 387–405 (1998).
14. G. Bodenhausen and R. R. Ernst, *J. Am. Chem. Soc.* **104,** 1304–1309 (1982).
15. S. Grzesiek and A. Bax, *J. Am. Chem. Soc.* **114,** 6291–6293 (1992).
16. M. Wittekind and L. Mueller, *J. Magn. Reson. Ser. B* **101,** 201–205 (1992).
17. A. Meissner and O. W. Sørensen, *J. Magn. Reson.* **150,** 100–104 (2001).
18. A. Meissner and O. W. Sørensen, *J. Magn. Reson.* **151,** 328–331 (2001).
19. A. M. Gronenborn, D. R. Filpula, N. Z. Essig, A. Achari, M. Whitlow, P. T. Wingfield, and G. M. Clore, *Science* **253,** 657–661 (1991).
20. T. J. Norwood, J. Boyd, and I. D. Campbell, *FEBS Lett.* **255,** 369–371 (1989).
21. A. Bax, M. Ikura, L. E. Kay, D. A. Torchia, and R. Tschudin, *J. Magn. Reson.* **86,** 304–318 (1990).
22. G. Wider, *Prog. Nucl. Magn. Reson. Spectrosc.* **32,** 193–275 (1998).
23. O. W. Sørensen, G. W. Eich, M. H. Levitt, G. Bodenhausen, and R. R. Ernst, *Prog. Nucl. Magn. Reson. Spectrosc.* **16,** 163–192 (1983).
24. G. Drobny, A. Pines, S. Sinton, D. Weitekamp, and D. Wemmer, *Faraday Div. Chem. Soc. Symp.* **13,** 49 (1979).
25. G. Bodenhausen, R. L. Vold, and R. R. Vold, *J. Magn. Reson.* **37,** 93–106 (1980).
26. R. R. Ernst, G. Bodenhausen, and A. Wokaun, "Principles of Nuclear Magnetic Resonance in One and Two dimensions," Chap. 7, Clarendon Press, Oxford (1987).
27. L. E. Kay, M. Ikura, R. Tschudin, and A. Bax, *J. Magn. Reson.* **89,** 496–514 (1990).
28. A. J. Shaka, J. Keeler, and R. Freeman, *J. Magn. Reson.* **53,** 313–340 (1983).
29. D. J. States, R. A. Haberkorn, and D. J. Ruben, *J. Magn. Reson.* **48,** 286–292 (1982).
30. F. Delaglio, S. Grzesiek, G. W. Vuister, G. Zhu, J. Pferfer, and A. Bax, *J. Biomol. NMR* **6,** 277–293 (1995).
31. S. Grzesiek and A. Bax, *J. Am. Chem. Soc.* **115,** 12593–12594 (1993).
32. M. Piotto, V. Saudek, and V. Sklenar, *J. Biomol. NMR* **2,** 661–665 (1992).
33. P. Koehl, *Prog. Nucl. Magn. Reson. Spectrosc.* **34,** 257–299 (1999).
34. K. Pervushin, P. Riek, G. Wider, and K. Wuthrich, *Proc. Natl. Acad. Sci. USA* **94,** 12366–12371 (1997).
35. S. B. Shuker, P. J. Hajduk, R. P. Meadows, and S. W. Fesik, *Science* **274,** 1531–1534 (1996).
36. P. J. Hajduk, E. T. Olejniczak, and S. W. Fesik, *J. Am. Chem. Soc.* **119,** 12257–12261 (1997).
37. P. J. Hajduk, D. J. Augeri, J. Mack, R. Mendoza, J. G. Yang, S. F. Betz, and S. W. Fesik, *J. Am. Chem. Soc.* **122,** 7898–7904 (2000).